Journal of
Water & Climate Change

IWA PUBLISHING

Journal of Water and Climate Change Vol 14 No 6, 1961 doi: 10.2166/wcc.2023.067

Flux and stable isotope fractionation of CO_2 in a mesic prairie headwater stream

Brock S. Norwood[a,b], Randy L. Stotler[c], Andrea Brookfield[c,*], Pamela L. Sullivan[d] and G. L. Macpherson[b]

[a] DHI Group, Inc., Denver, CO.
[b] Geology Department, University of Kansas, Lawrence, KS, USA 66045
[c] Department of Earth and Environmental Sciences, University of Waterloo, Waterloo, Ontario, Canada N2L 3G1
[d] College of Earth, Ocean and Atmospheric Science, Oregon State University, OR 97331, USA
*Corresponding author. E-mail: andrea.brookfield@uwaterloo.ca

RLS, 0000-0001-9893-9259; AB, 0000-0003-3739-0025; PLS, 0000-0001-8780-8501; GLM, 0000-0001-7461-2788

ABSTRACT

The carbon dioxide (CO_2) fluxes from headwater streams are not well quantified and could be a source of significant carbon, particularly in systems underlain by carbonate lithology. Also, the sensitivity of carbonate systems to changes in temperature will make these fluxes even more significant as climate changes. This study quantifies small-scale CO_2 efflux and estimates annual CO_2 emission from a headwater stream at the Konza Prairie Long-Term Ecological Research Site and Biological Station (Konza), in a complex terrain of horizontal, alternating limestones and shales with small-scale karst features. CO_2 effluxes ranged from 2.2 to 214 g CO_2 m^{-2} day^{-1} (mean: 20.9 CO_2 m^{-2} day^{-1}). Downstream of point groundwater discharge sources, CO_2 efflux decreased, over 2 m, to 3–40% of the point-source flux, while δ^{13}C-CO_2 increased, ranging from −9.8 ‰ to −23.2 ‰ V-PDB. The δ^{13}C-CO_2 increase was not strictly proportional to the CO_2 flux but related to the origin of vadose zone CO_2. The high spatial and temporal variability of CO_2 efflux from this headwater stream informs those doing similar measurements and those working on upscaling stream data, that local variability should be assessed to estimate the impact of headwater stream CO_2 efflux on the global carbon cycle.

Key words: CO_2, CO_2 efflux, headwater stream, merokarst, stable carbon isotopes

HIGHLIGHTS

- An intermittent stream in merokarst terrain has highly variable efflux both spatially and temporally.
- CO_2 efflux was rapid: 2 m downstream of the point of groundwater discharge flux was 3–40% of the point-source flux.
- δ^{13}C-CO_2 correlated negatively with CO_2 fluxes except for two high-flux values, suggesting δ^{13}C-CO_2 is not a reliable indicator of CO_2 flux.

1. INTRODUCTION

Headwater stream emission of carbon dioxide (CO_2) is a significant part of the short-term carbon cycle (Cole *et al.* 2007, 2010; Nadeau & Rains 2007; Battin *et al.* 2009; Alin *et al.* 2011; Butman & Raymond 2011; Striegl *et al.* 2012; Atkins *et al.* 2013; Dinsmore *et al.* 2013; Hotchkiss *et al.* 2015; Schade *et al.* 2016; Marx *et al.* 2017; Horgby *et al.* 2019; Li *et al.* 2021). Headwater streams are complex environments, accounting for more than half of all stream lengths globally (Nadeau & Rains 2007). The small-scale heterogeneity common in these systems makes it difficult to characterize and upscale CO_2 cycling and to quantify their contributions to atmospheric greenhouse gas concentrations. Further, recent research has highlighted the importance of karstic springs, and their contributions to headwater environments, as CO_2 sources to the atmosphere (Maas & Wicks 2017; Lee *et al.* 2021).

Carbon flux from streams depends on terrestrial production and storage of CO_2 in the soil and in shallow aquifers, and on the hydrogeologic pathways that connect them, in addition to in-stream CO_2 production (Bernal *et al.* 2022). Groundwater discharge is the primary source of dissolved gases in low-order streams (Hope *et al.* 2001; Doctor *et al.* 2008; Johnson *et al.* 2008; Sand-Jensen & Staehr 2012; Crawford *et al.* 2013; Hotchkiss *et al.* 2015; Deirmendjian *et al.* 2018), with shallow aquifers and interflow, not deep groundwater, the main contributors of CO_2 to streams (Hotchkiss *et al.* 2015). It is estimated that over 70% of this CO_2 stream flux is produced terrestrially, with the majority of the terrestrial contribution derived from

infiltration through soil (Hotchkiss *et al.* 2015; Nosrati *et al.* 2020). Terrestrially derived CO_2 is produced during organic matter degradation, and root and organism respiration. Meteoric water infiltrates the soil, taking up soil CO_2 (Chapelle 2000). Although most soil CO_2 escapes upward to the atmosphere, downward water migration to groundwater dissolves and transports ~1–2% of soil CO_2 (Hendry *et al.* 1993; Schlesinger & Lichter 2001; Tsypin & Macpherson 2012). Carbonic acid from the dissolution of CO_2 dissolves carbonate minerals, releasing inorganic carbon into the solution. These carbon fluxes lead to the accumulation of CO_2 in groundwater, with concentrations one to two orders of magnitude higher than in the atmosphere (Schlesinger & Melack 1981; Johnson *et al.* 2008; Macpherson *et al.* 2008; Macpherson 2009; Monger *et al.* 2015; Macpherson & Sullivan 2019). When groundwater discharges into surface water, gas efflux is driven by the concentration gradient between the water and atmosphere.

Given the extensive distribution of carbonate terrains across the world (Weary & Doctor 2014; Chen *et al.* 2017), the sensitivity of carbonate weathering to changes in temperature and water residence time (Sullivan *et al.* 2019), and the complexity of groundwater–surface water interactions, it is necessary to better quantify CO_2 efflux in carbonate-hosted headwaters. In addition, it is critical to relate the CO_2 flux to groundwater discharge to understand its contribution to global greenhouse gases. We present the results of a ~1-year study of a headwater stream at the Konza Prairie Long-Term Ecological Research Site (LTER) and Biological Station (Konza), where merokarst (thin limestones alternating with shales) presents both the opportunity and challenge to characterize point sources of groundwater discharge (herein referred to as point sources) and resulting CO_2 efflux. We contrast the CO_2 fluxes from the stream water passing over outcrops or subcrops of limestone and shale, quantify the stream CO_2 emission within the lower half of the watershed (~1.1 km stream length), and test how efflux is related to δ^{13}C-CO_2.

2. FIELD SITE

The Konza LTER is part of one of the last remaining undisturbed, tallgrass prairies in North America. The 3,487-ha research area is located in the Flint Hills, near Manhattan, Kansas (Figure 1(a)). The Flint Hills, unlike other prairie environments, lack soils suitable for tilling, which has reduced anthropogenic stresses on the ecosystem. Konza LTER is divided into 60 watersheds with different research treatments; Tsypin & Macpherson (2012) showed that the study watershed, N04d (1.2 km^2), is on a major watershed divide and is surrounded by grazed land. Stream reaches in watershed N04d are intermittent except for a few small pools that are dry only during the most severe droughts (Figure 1).

2.1. Climate

Konza has a temperate, mid-continental climate (Hayden 1998), with high variability both seasonally and annually (Nippert & Knapp 2007). From 1983 to 2016 (Nippert 2017), the average daily air temperature at Konza was 12.8 °C, and the mean total annual precipitation was 839 mm. From July 2015 to August 2016, the period of this study, the average air temperature was 14.9 °C and precipitation was 974 mm (116% of the annual mean precipitation; Supplemental Table S1); 70% of precipitation fell during the growing season (March to October). On an annual basis, both 2015 and 2016 exceeded both the long-term average precipitation and air temperature.

2.2. Vegetation

Konza lies along the southeastern margin of the North American Prairie (Hayden 1998). Konza flora is dominated by C_4 grasses and forbs (C_3), while woody vegetation (C_3) is found in patches in riparian zones and on hillslopes (Veach *et al.* 2014). C_3 and C_4 plants differ in their method of carbon fixation during photosynthesis (Wang *et al.* 2012), which affects the δ^{13}C of CO_2 produced during the breakdown of the plants.

2.3. Geology

Konza is underlain by thin soils and merokarst. The loess-based soils, primarily silty clays and silty clay loams (NRCS 2006), are thickest (~1 m) at the base of slopes and patchy on the plateaus (Ranson *et al.* 1998). The merokarst is thin, interlayered beds of Lower Permian age limestones (mostly 1–2 m) and thicker shales (4–6 m; Supplemental Figure S1); discontinuous Quaternary alluvium occupies valleys. Bedrock strikes northeast-southwest and dips ~2° northwest (Twiss 1988). Limestone outcrops form flat uplands and benches along the hillsides; slopes form over shales. Streams dissect the landscape into relatively steep-sided valleys (Macpherson 1996). The limestones and alluvium act as aquifers and shales as aquitards; many of the limestones are hydraulically connected to the streams (Macpherson *et al.* 2008; Hatley *et al.* 2023). Hydraulic

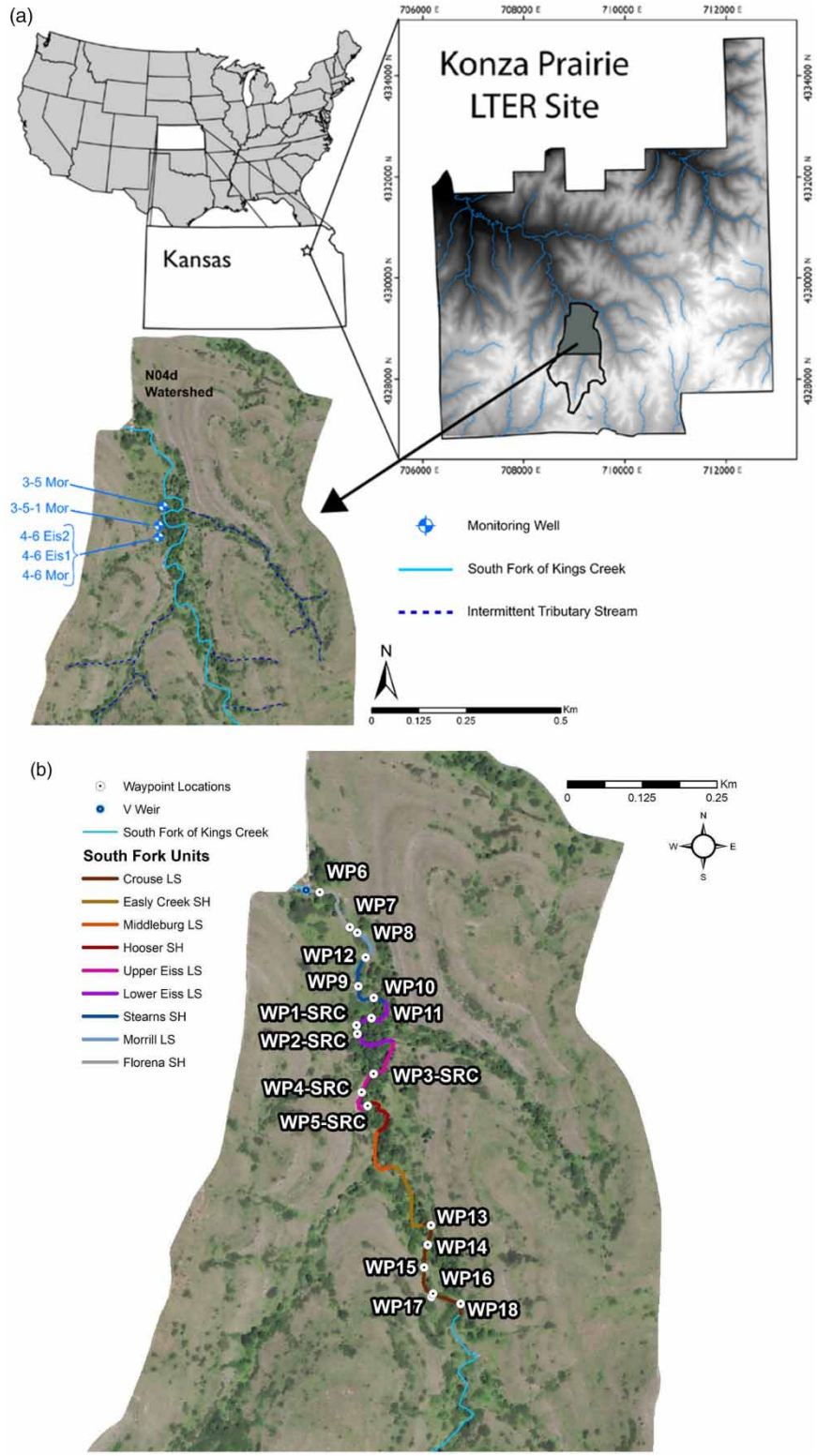

Figure 1 | (a) Location map of the Konza Prairie LTER Site with inset of the N04d watershed. Data from monitoring wells are included in Supplemental Information. (b) Waypoint (WP) GPS locations and stream reach discretization based on geology along the South Fork of Kings Creek. SRC: point-source location. Some downstream sampling locations are 1 and 2 m from SRC locations, so are not resolved on this scale map and are labeled with a single WP. Stream flows north. WP 17 is a spring ~5 m above the streambank.

conductivities of the limestones, controlled by secondary porosity, range over five orders of magnitude (10^{-8} to 10^{-3} m s^{-1}; Pomes 1995; Sullivan *et al.* 2020).

3. METHODS

Geologic mapping, measurement sites, and sampling sites spanned 1,125 m of the South Fork of Kings Creek and were located with a Garmin Etrex Legend GPS. Stream segments were discretized, based on geology, into nine reaches (Figure 1(b)). Those underlain by shale and limestone account for 41 and 59% of the total stream length, respectively. Stream reaches underlain by shale are narrower than reaches underlain by limestone; for calculation purposes, widths of stream reaches underlain by shale were set at 1.0 m and those by limestones at 1.5 m. For the sake of brevity, units will be identified with their simplified geologic name: Crouse, Upper Eiss, Lower Eiss, Stearns, Morrill, and Florena.

To quantify the flux and fractionation of CO_2 in this system, measurements of stream discharge were made, water samples were collected and analyzed for basic water chemistry and for C isotopes, and CO_2 flux was measured in the stream. As this is an intermittent, flashy, stream, sampling was not possible when there was no water in the stream and also when the flows were so high as to be unsafe for sampling.

3.1. Stream and point discharge

Stream discharge was measured using data from the triangular-throated weir, and point discharge measurements were taken at nine WP locations on two different days using a ~30 cm long, 0.25 cm inside-diameter pitot tube. Streamflow measurements follow protocols outlined by the Environmental Protection Agency (Meals & Dressing 2008) and the United States Geological Survey (USGS 2016).

Throughout most of the year, temperature differences exist between groundwater (Macpherson 2020) and surface water (Brookfield *et al.* 2017; Nippert 2017; Nippert & Knapp 2007) at Konza. The average groundwater temperature was ~16 °C for the study period, with the average surface water temperature of ~21 °C. This temperature differential permitted the location of point-source groundwater discharge locations (point sources) by a FLIR® T600 Thermal Imaging Infrared Camera (FLIR Camera). Seeps and springs flowing from fractures along the streambank and streambed were observed, and they were underlain by the Morrill, Eiss, and Crouse limestones. These point sources were used to evaluate degassing lengths.

3.2. Water chemistry

Groundwater and stream water samples were collected over the study period. Groundwater was sampled from five observation wells: 3-5 Mor, 3-5-1 Mor, 3-6 Mor, 4-6 Eis1, and 4-6 Eis2 (Figure 1(a)). The results of chemical analysis (inorganic species and pH; Norwood 2020) were used to calculate aqueous pCO_2 by developing with PHREEQC Interactive 3.1.7–9213 (Charlton *et al.* 1997; Supplemental Table S2). Charge balances were also calculated using PHREEQC.

3.3. CO_2 flux and carbon isotopes

CO_2 efflux from the stream was measured with a suspended chamber (Crawford *et al.* 2014; Rawitch *et al.* 2019). Two chamber designs were lab tested (Norwood 2020) and used in the field. The first is a 3D-printed ABS plastic rectangular prism with rounded, triangular prisms on the front and back for streamlining; it has a small footprint (9.40×10^{-3} m^2) and was sealed with acetone vapor. The second is made with 5-mm thick plexiglass, is heavier, has the shape of a rectangular prism, and has a larger footprint (1.55×10^{-2} m^2).

For each trial, the bottom of the chamber was submerged ~2 cm below the water surface, sealing the chamber to the water surface and preventing the influx of atmospheric CO_2. The chamber was connected to a pump and a Li-Cor LI-820 CO_2 Infrared Gas Analyzer using Tygon® tubing; the circulating air (1 L/min) passed through a Drierite® filter to remove moisture. CO_2 concentrations from the chamber were logged at 1-s intervals; pressure changes in the chamber were minimized by returning analyzed gas to the chamber. Chamber trials lasted at least 5 minutes, ensuring that the CO_2 emission rate became linear. Between trials, the chamber atmosphere was allowed to equilibrate with the atmosphere. Atmospheric CO_2 (ppm), temperature (°C), and relative humidity (RH, %) were measured using an AZ-77535 CO_2/temperature/RH meter.

Chamber flux (F_c) was calculated for each suspended chamber measurement as follows:

$$F_c = \left(\frac{d(CO_2)}{dt}\right)\left(\frac{p * V_c}{R * T * A_c}\right) \quad (1)$$

where $(d(CO_2)/dt)$ is the change in chamber CO_2 concentration with time, p is the gas pressure in the chamber, V_c is the chamber volume, R is the universal gas constant, T is the air temperature in Kelvin, and A_c is the surface area of water covered by the chamber (Müller *et al.* 2015). To determine $(d(CO_2)/dt)$, a linear regression was fit to the linear portion of the flux data; data were excluded if $R^2 < 0.90$. The diffusive transfer of gases between a water surface and the atmosphere (F; $[ML^{-3}T^{-1}]$) is expressed as follows:

$$F = k(C_w - C_{atm}) \tag{2}$$

where C_{atm} is the atmospheric gas concentration above the water body, C_w is the gas concentration in the water, and k is the gas transfer coefficient (MacIntyre *et al.* 1995). The gas transfer coefficient (gas transfer velocity) is temperature and density dependent (Demars & Manson 2013; Wanninkhof 2014). k is converted to k_{600} (Cole & Caraco 1998) to compare with other gas transfer rates at 20 °C.

To estimate the flux from the stream, we first calculated an estimate of total daily flux (F_{TD}) (g CO_2 day^{-1}) using average flux for each stream reach as follows:

$$F_{TD} = \sum (F_{SU} * A_{SU}) \tag{3}$$

F_{SU} is the daily flux (g CO_2 m^{-2} day^{-1}), and A_{SU} is the surface area (m^2) for each stream reach. For six of the stream reaches, average CO_2 flux was calculated using direct measurements. For two of the units where direct measurements were not made, and mean CO_2 flux (mol m^2 day^{-1}) was used for each rock type (shale or limestone). CO_2 flux from the Florena was only measured once, so that measurement was used to represent that unit. An estimate of total flux for the study period (F_{SP}) was then determined by:

$$F_{SP} = F_s * t \tag{4}$$

where t is days of recorded stream discharge at the triangle-throated flume (weir) at the northwestern end of the watershed (Figure 1).

Gas was sampled directly from the suspended chamber and stored in 0.5 L Tedlar® Gas-Sampling Bags for C isotope determination. These samples were analyzed on a Picarro® G2201-I Analyzer for Isotopic CO_2/CH_4 to determine $\delta^{13}C$-CO_2. Two reference standards for CO_2 gas ($\delta^{13}C$ of −40.78‰ and −10.42‰, V-PDB) were used along with CO_2 gas standards (500 ppm and 1,000 ppm) for calibration. Samples were injected directly into the Picarro analyzer from the gas-sampling bags. Between analyses, nitrogen gas flushed the Picarro of CO_2.

4. RESULTS

4.1. Stream and point discharge

The Konza LTER Program records stream discharge at the weir every 5 min; data are transformed into daily averages (Dodds 2021). The discharge measurements at the weir are assumed to be a reliable indicator of upstream flow in N04d; however, we also recorded discharge at upstream reaches on two dates when there was no flow at the weir. Over the study period, discharge was recorded at the weir 68% of the time. The mean discharge was 138 m^3/day, and the median discharge was 402 m^3/day (Supplemental Figure S2). The mean discharge and sum of daily discharge from 1 January 2016 to 2 August 2016 were almost twice as high as in 2015 (Supplemental Table S1).

Chamber-site discharge measurements were made to supplement weir data on two different days with a pitot tube. Measure values varied over an order of magnitude, and measurement points were ~50 to ~100 m apart (Figure 2). The upstream-most reach is underlain by the Crouse and was measured on 2 August 2016. Most other locations are also underlain by limestone, except WP-10B (Stearns), and were measured on 22 July 2016. Note that no discharge was recorded at the weir on either of those days, illustrating that this is a losing stream.

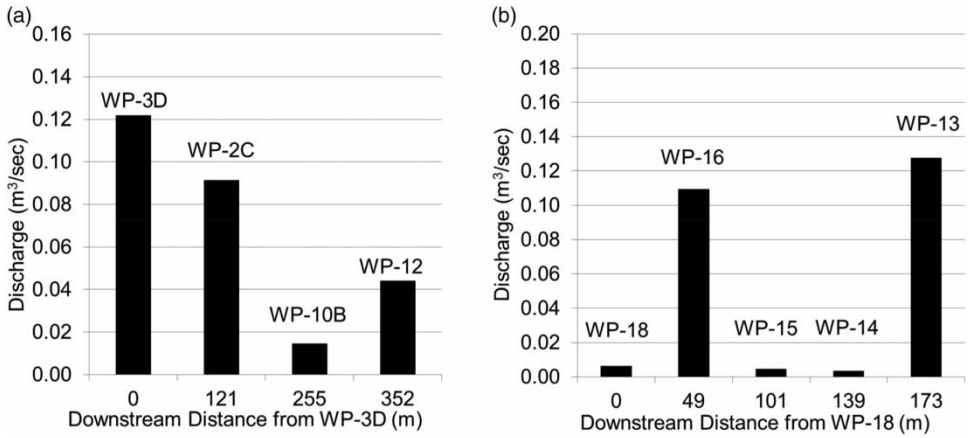

Figure 2 | Stream discharge measured with downstream distance from (a) WP-18 (Crouse, 2 August 2016) and (b) WP-3D (Upper Eiss, Lower Eiss, Stearns, and Morrill, 22 July 2016).

4.2. Water chemistry

Groundwater and surface water samples were collected over the 379 days between 21 July 2015 and 2 August 2016 (Supplemental Table S3). Charge balances are less than 5% for all but three analyses. Water chemistry is typical of limestone terrains, dominated by calcium and bicarbonate with slightly alkaline pH and moderate total dissolved solids. Analytical methods and results are similar to other studies done at the site (e.g., Macpherson 1996; Macpherson *et al.* 2008; Macpherson & Sullivan 2019). With the exception of seasonal variations in temperature and nitrate, very little spatial or temporal variability was observed at this site (Table 1) and is not further discussed.

4.3. CO_2 flux and carbon isotopes

Carbon flux measurements from the South Fork ranged from 2.2 to 214 g CO_2 m^{-2} day^{-1}, with a mean CO_2 flux of 20.9 g CO_2 m^{-2} day^{-1} $\pm$ 41.4 g CO_2 m^{-2} day^{-1} (1 S.D.; Supplemental Table S4). WP-3A-SRC and WP-17 are high-flux outliers. For nearly all locations, flux measurements were higher for stream reaches underlain by limestone than those underlain by shale. The CO_2 fluxes measured in the three limestone units also varied, even between the more-permeable (Upper Eiss) and less-permeable (Lower Eiss) portions of the same limestone member (Table 2 and Supplemental Table S4). During

Table 1 | Average and standard deviation (in brackets) of water chemistry in groundwater and surface water samples

	Sampling location					
	3-5 Mor	3-5-1 Mor	4-6 Eis2	4-6 Eis1	4-6 Mor	Surface water
Temperature (°C)	15.8 (2.07)	15.4 (1.54)	16.6 (1.76)	16.6 (1.88)	16.0 (2.25)	22.1 (5.82)
Ca (mg/L)	102.2 (10.21)	86.7 (1.34)	91.0 (5.62)	71.1 (2.58)	102.1 (6.48)	93.2 (9.43)
Mg (mg/L)	20.8 (2.06)	28.4 (0.35)	15.4 (2.54)	26.9 (0.93)	23.4 (1.67)	20.4 (1.85)
Na (mg/L)	5.0 (0.49)	2.9 (0.46)	3.8 (0.53)	6.7 (0.83)	5.4 (0.41)	3.3 (0.99)
K (mg/L)	1.0 (0.21)	1.2 (0.05)	0.75 (0.21)	1.2 (0.15)	1.2 (0.36)	1.1 (0.24)
Si (mg/L)	6.6 (1.48)	6.0 (0.44)	5.8 (1.49)	6.6 (0.58)	6.5 (0.58)	5.3 (0.68)
Cl (mg/L)	2.6 (1.05)	30 (0.68)	2.0 (0.49)	2.1 (0.33)	2.7 (0.48)	2.5 (0.77)
Alkalinity (meq/L)	406.9 (26.09)	380.3 (2.49)	353.5 (16.87)	348.8 (16.32)	401.0 (23.37)	359.8 (34.22)
SO_4 (mg/L)	30.7 (12.73)	41.5 (1.90)	12.9 (3.75)	23.0 (1.76)	34.2 (9.99)	29.3 (4.75)
NO_3-N (mg/L)	0.0 (0.02)	0.0 (0.05)	0.1 (0.05)	0.01 (0.07)	0.0 (0.03)	0.1 (0.11)
pH	7.2 (0.13)	7.3 (0.09)	7.2 (0.08)	7.5 (0.14)	7.3 (0.11)	7.8 (0.41)

the study period, the variability within a geologic unit, measured two to four times, was higher in high permeability units (Upper Eiss; Crouse [presumed high because of frequency of springs in this unit; Barry 2018]) than low permeability units (Lower Eiss, Stearns, Morrill). Among the limestones, the CO_2 fluxes and the coefficients of variation of the CO_2 fluxes decreased with unit thickness (Table 2). Point sources were not found in stream reaches underlain by shale.

To investigate degassing lengths, measurements were made at the point source and at 1 and 2 m downstream. In the Upper Eiss reach, carbon flux at 2 m downstream from the point source ranged from 14 to 42% of the point-source flux, decreasing in all trials (Figure 3). Location WP-1 (Lower Eiss) had multiple rather than a single-point source within the 2-m distance, resulting in nonuniform downstream fluxes. In the Upper Eiss reach, CO_2 flux ranged from ~7 to 214 g CO_2 m^{-2} day^{-1}, the high value being an outlier; the Crouse spring located just west of the stream was the other high-flux outlier (Supplemental Table S4). Figure 3 shows the trials where the groundwater discharge was measured directly, without the influence of stream water. This was accomplished using a ~0.3 m diameter half-pipe made of aluminum flashing and plastic sheeting to isolate the point-source water (location WP3, measured twice on the same day) and when there was no upstream flow (WP4). The WP-3 and WP-4 fluxes were similar, suggesting that the isolation method was successful. The data in the lower hydraulic conductivity Morrill reach and the long Crouse reach (Supplemental Table S4) have irregular degassing patterns similar to the Lower Eiss reach.

Table 3 presents the mean CO_2 flux for each geologically constrained stream reach (stream reaches that correspond to only one geologic unit) during the 379-day study period. The average flux for all units was of the same order of magnitude with or without outliers: 14.5 ± 14.8 g CO_2 m^{-2} day^{-1} with and 10.2 ± 10.6 g CO_2 m^{-2} day^{-1} without outliers. Therefore, during the approximately 1-year study period, the South Fork emitted between 4.2 and 7.0 metric tons of CO_2 from the stream to the atmosphere.

Stable carbon isotope ratios of chamber CO_2 (δ^{13}C-CO_2) ranged from −9.7 ‰ to −23.2 ‰ (V-PDB) with a mean of −14.9 ±4.2‰ (V-PDB) (Supplemental Table S3). Gas samples collected at point sources have lower isotopic compositions (mean, −16.8 ±3.0‰ V-PDB) than stream reaches with minimal groundwater influence (mean, −10.5 ±0.4‰ V-PDB). Similar to CO_2 flux, small-scale spatial trends in δ^{13}C-CO_2 showed a consistent depletion in ^{12}C from point source to downstream (Figure 4).

Table 2 | Variability in CO_2 flux measurements in CO_2 m^{-2} day^{-1} taken at same locations but different times

Measurement location		Mean	Standard deviation	Coefficient of variation %	Count
All with multiple measurements					
Crouse LS, WP-13		14.2	13.4	95	2
Upper Eiss LS, WP-4	SRC	14.1	16.3	116	2
Upper Eiss LS, WP-3	SRC	57.1	88.4	155	5
	1 m DS	35.8	18.5	52	3
	2 m DS	17.6	10.5	59	3
Lower Eiss LS, WP-2	SRC	13.1	4.6	35	2
	1 m DS	10.1	4.8	47	2
	2 m DS	7.3	1.4	19	3
Lower Eiss LS, WP-1	SRC	11.2	1.5	14	2
	1 m DS	13.7	0.2	1	2
	2 m DS	14.5	7.6	53	2
Morrill LS, WP-7		4.3	0.5	11	2
Without outliers					
Upper Eiss LS, WP-3	SRC	17.8	12.1	68	4
	1 m DS	25.1	0.5	2	2
	2 m DS	11.6	0.1	1	2

SRC, point source of groundwater discharge; DS, downstream of point source.

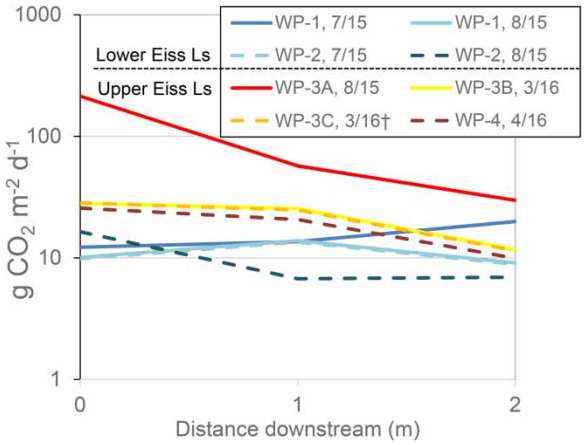

Figure 3 | CO_2 flux changes with downstream distance from point source.

5. DISCUSSION

5.1. Spatial and temporal variability of CO_2 flux

The spatially and temporally variable CO_2 fluxes and carbon isotopes in this study reflect the geomorphologic and hydrologic heterogeneity of the South Fork, variable annual weather patterns, and vegetation. Point sources were only identified in reaches underlain by limestone and at geologic contacts between limestones and shales.

The spatial variation of CO_2 flux along the South Fork is attributed to point sources of groundwater discharge. In addition, the highest daily CO_2 emissions corresponded to the thickest (Crouse) and most permeable (Upper Eiss) limestones (Figure 3; Supplemental Table S4). Where measurements were made downstream of the point source, most locations showed a large decline in CO_2 efflux (Figure 3; Supplemental Table S4), reinforcing the complexity of characterizing the contribution of degassed CO_2. In some stream reaches, multiple point sources occur over short distances, further increasing the complexity of the degassing patterns (e.g., WP-1, Lower Eiss). These short distances are in contrast to the previous work that evaluated degassing over stream lengths of 100 s–1,000 s of meters (e.g., Mohammadi *et al.* 2020). In the Morrill reach, the discharge and degassing patterns may also be complicated by complex groundwater flow patterns. This includes groundwater moving upstream with respect to surface water flow, which then discharges below the weir, suggesting losing stream behavior

Table 3 | CO_2 properties of stream reaches underlain by geologic units

Stream segment[a]	Mean k600 (m/s)	Mean flux (g CO_2/m^2/day)[b]	Stream length (m)	Stream width (m)	Stream area (m^2)	Flux (g CO_2/day)[b]
Crouse LS	5.81×10^{-8}	35.7/9.18	201	1.5	302	10,771/2,773
Easly Creek SH	1.08×10^{-8}	3.48	131	1.0	131	456
Middleburg LS	2.55×10^{-8}	34.61	87	1.5	130	4,499
Hooser SH	1.08×10^{-8}	3.48	85	1.0	85.3	297
Upper Eiss LS	1.81×10^{-8}	31.7/19.5	154	1.5	231	7,321/4,512
Lower Eiss LS	7.07×10^{-9}	10.8	162	1.5	243	2,614
Stearns SH¥	1.13×10^{-8}	4.46	119	1.0	119	531
Morrill LS	2.22×10^{-8}	4.15	61	1.5	91.1	378
Florena SH	1.08×10^{-8}	2.51	126	1.0	126	316
Total stream length (m) and stream area (m^2)			1,125		1,458	

[a]LS, limestone; SH, shale; informal names. See Supplemental Figure S1 for full stratigraphic names.
[b]Where two values are entered, the first includes high-flux outliers and the second excludes them.

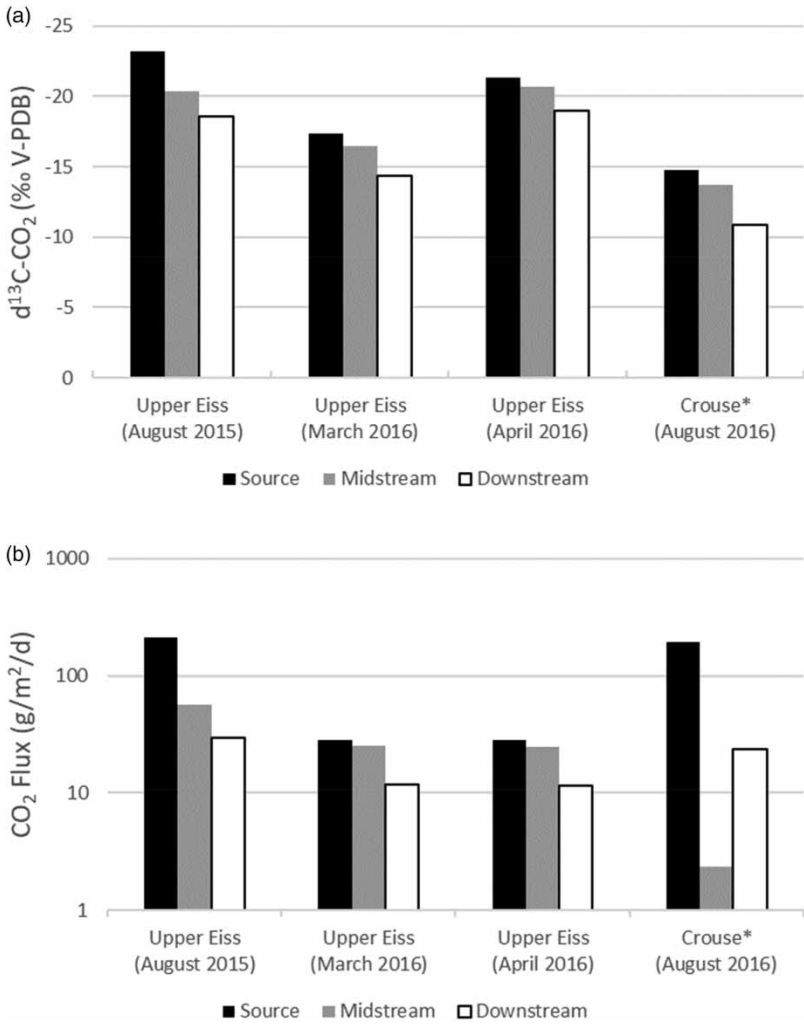

Figure 4 | Changes in (a) δ^{13}C-CO_2 and (b) flux with distance downstream from point sources in Eiss and Crouse limestones. In each set of three, measurements are at point source and two locations downstream from the point source. In Eiss limestone, midstream and downstream represent 1 and 2 m downstream of point source, respectively. In Crouse limestone, source is at spring outlet 2 m from stream, and midstream and downstream are measured at WP-14 and WP-13. Datasets of August 2015 and March 2016 for the Upper Eiss limestone are the same locations; the April 2016 location is ~50 m upstream.

(Sullivan *et al.* 2020, their supplemental information; Barry 2018); and small-scale gaining and losing stream behavior within the outcrop in the stream (Norwood 2020). The extensive outcrop of the Crouse in the upstream portion (Figure 1(b) and Table 3) has multiple point sources with different CO_2 fluxes (Supplemental Table S4): the highest CO_2 flux corresponds to a spring located just west of the stream and the second highest to the Crouse Limestone-Easly Creek Shale boundary, suggesting the importance of less-permeable units forcing groundwater discharge.

As a simplified analysis of this data, we consider the rate of changes in fluxes downstream of point sources in the same manner as one would consider the half-life of radioactive decay. We calculate these 'decay rates' using measurements provided at 1 and 2 m downstream of the point sources measured in the Eiss Limestone and assume a linear decay of the natural logarithms of the measurements, as the nature of the decay rate is not known. However, the measured data fit the linear functions with coefficients of determination of 0.96, 0.84, and 0.86, for August 2015, March 2016, and April 2016 measurements, respectively. We do not consider the Crouse Limestone due to the previously mentioned complexities in this thicker limestone unit. Using the values for the Eiss Limestone in Figure 4(b), the distance to reduce the CO_2 flux by half for August 2015, March 2016, and April 2016 were 0.70 m, 1.57 m, and 1.54 m, respectively. It appears that this rate is dependent upon the initial flux rate at the point-source location, where a higher initial flux results in a shorter distance

to reduce that flux by half. This analysis is clearly limited by the few data points and measurement locations, but we feel it provides an interesting direction for future research.

Repeat measurements at the same locations demonstrate the variability in CO_2 flux at this site (Figure 3 and Table 2). Others have documented stream CO_2 content that may be strongly influenced by diurnal, seasonal, and annual factors (e.g., Hotchkiss *et al.* 2015; Marx *et al.* 2018). We propose that flux variability results from variations in hydraulic connectivity, as well as weather-driven recharge and groundwater flow directions, which is consistent with the recent work by Duvert *et al.* (2018). Table 2 shows the variability in measurements for all locations where at least two measurements were made. For measurements in limestones with lower hydraulic conductivity (Morrill, Lower Eiss), coefficients of variation of CO_2 flux are lower (1–53%) than those for limestones with higher hydraulic conductivity (Upper Eiss, Crouse; 52–155%).

An observed inverse relation between annual stream discharge and CO_2 efflux (Figure 5) suggests a link to watershed recharge dynamics, with less recharge allowing buildup of soil and/or groundwater CO_2 and subsequent discharge to the stream resulting in higher CO_2 efflux. The variation in groundwater CO_2 (Macpherson *et al.* 2008), where highest CO_2 occurs from September to November and lowest in February to April, is not reflected in the stream CO_2 efflux data we collected. A systematic investigation of temporal trends in stream CO_2 efflux seems necessary to relate seasonal groundwater CO_2 levels to flux data at point sources along the stream. This is consistent with the recent work by Wallin *et al.* (2020), which linked stream intermittency with variations in CO_2 dynamics. Note that because the aquifers at this site are limestones, the stream can be gaining or losing depending on recent recharge: at the high stream stage, the degassed stream water will enter the aquifer at the point sources and then later discharge within the same geologic unit at low stream stage (e.g., Pomes 1995; Macpherson & Sophocleous 2004), further complicating interpretation of CO_2 flux dynamics. This phenomenon is likely not unique to karst systems, but is possible whenever there are large changes in the stream stage (Winter *et al.* 1998).

The k_{600} values ranged over two orders of magnitude, from ~0.0002 to ~0.02 m d^{-1} (Supplemental Table S4). Excluding the highest k_{600}, which was measured at the Crouse spring (WP-17), the range lowers to one order of magnitude (~0.0002 to ~0.008), within the range of other k_{600}'s measured in other headwater streams with low stream velocities (e.g., Rawitch *et al.* 2021).

5.2. Spatial and temporal variability of δ^{13}C-CO_2

During the 2-m trials, most gas samples showed an inverse relationship between δ^{13}C-CO_2 and CO_2 flux (Figures 3 and 4). Over the 2-m distance downstream of point sources, isotopic signatures are higher by ~5–7‰ (Figure 4). Many have proposed that carbon isotope exchange with atmospheric CO_2 ($\delta^{13}C \sim -8$‰) is partly responsible for increasing downstream δ^{13}C values measured in streams and rivers (Taylor & Fox 1996; Yang *et al.* 1996; Atekwana & Krishnamurthy 1998; Karim & Veizer 2000; Hélie *et al.* 2002; Mayorga *et al.* 2005). However, isotopic equilibrium between dissolved CO_2 and atmospheric CO_2 can only be attained after the equilibrium of CO_2 concentration between atmosphere and stream/river water (Doctor *et al.* 2008). Thus, if a drive for CO_2 flux from water to the atmosphere exists, as observed in this study, fractionation of δ^{13}C-CO_2 will be primarily affected by gas efflux, rather than the carbon isotope exchange that accompanies carbon mixing. The observed depletion in ^{12}C during degassing therefore supports the hypothesis proposed by Doctor *et al.*

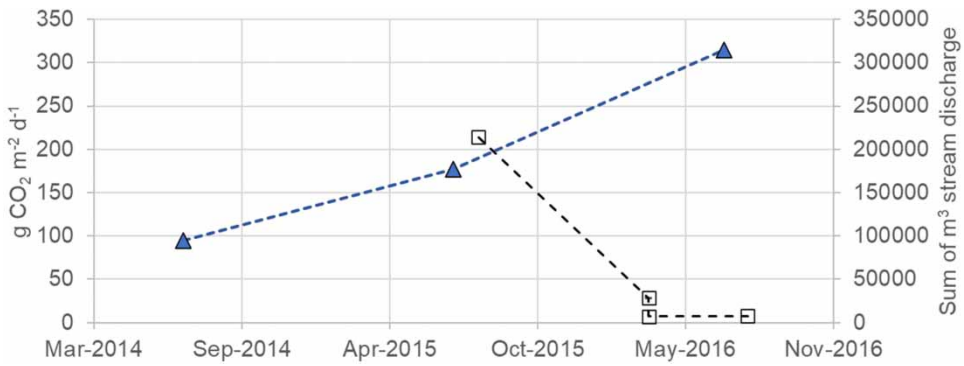

Figure 5 | Sum of annual stream discharge (filled triangles, plotted at mid-year dates) and CO_2 flux (open squares) measured multiple times at one location (WP-3) on the stream. The higher March 2016 flux represents the average of two measurements taken on a single day; coefficient of variation for that dataset is 3%, which is smaller than the symbol size.

(2008) and Venkiteswaran *et al.* (2014) that fractionation in the isotopic composition of DIC or CO_2 is driven by the process of gas transfer from stream to atmosphere, rather than mixing of CO_2 between the stream and atmosphere.

With two exceptions, CO_2 efflux rates show moderate ($R^2 = 0.4$ to 0.6) negative Pearson correlation coefficients with δ^{13}C-CO_2 (Figure 6; $R^2 = 0.5$, $p < 0.0001$); the exceptions are two events with the highest flux rates. This lack of overall correlation indicates that the flux rate is an unreliable predictor of δ^{13}C-CO_2, particularly when high-flux rates are present. This contrasts with the results from a sandy lowland watershed with more continuous groundwater discharge (Deirmendjian & Abril 2018) and indicates that the ability of the flux rate to predict δ^{13}C-CO_2 has upper limits on the flux rate used.

We propose that the δ^{13}C-CO_2 at point sources is controlled by processes other than the flux rate. We suggest the controls include the supply of CO_2 to groundwater from soil (e.g., Andrews & Schlesinger 2001; Kessler & Harvey 2001; Macpherson *et al.* 2008; Tsypin & Macpherson 2012), vegetation type, variation in precipitation and streamflow, and degree of interaction with the limestone aquifers. The main sources of soil CO_2 are root respiration and microbial oxidation of organic C (Kuzyakov & Domanski 2000; Cisneros-Dozal *et al.* 2006; Wen *et al.* 2021). Thus, δ^{13}C-CO_2 in the soil atmosphere should reflect overlying vegetation. At this site, there are both C_3 plants (generally −27‰) and C_4 plants (generally −13‰); their isotope ratio is also affected by the moisture content, temperature (Brown *et al.* 2009), recharge timing (Brookfield *et al.* 2017), and other factors related to vegetation functioning (e.g., Cernusak *et al.* 2013). The δ^{13}C-CO_2 in stream gas samples, for those closest to the point sources, should relate to groundwater δ^{13}C-DIC, groundwater travel distance (degree of reaction with the limestone), and nearby vegetation type assuming soil CO_2 continues to be added to groundwater as it approaches the stream (Figure 7). Enrichment in ^{13}C caused by dissolved CO_2 reacting with the marine limestone aquifer material will have the greatest effect on δ^{13}C in the groundwater that has traveled longer distances and moves slower (low-hydraulic conductivity units or lower hydraulic conductivity portions of units). At the study site, a mixture of woody plants and grasses are found above and near the Crouse Limestone, Stearns Shale, and Morrill Limestone reaches, while

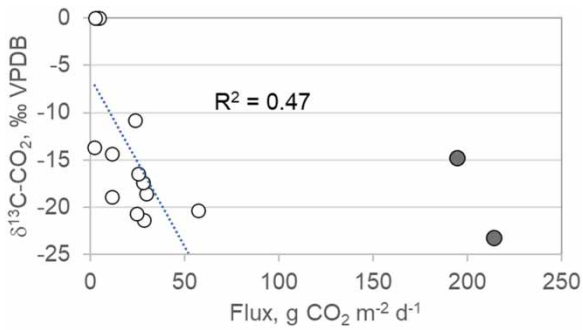

Figure 6 | All but the two highest flux measurements show a significant, negative correlation with δ^{13}C-CO_2.

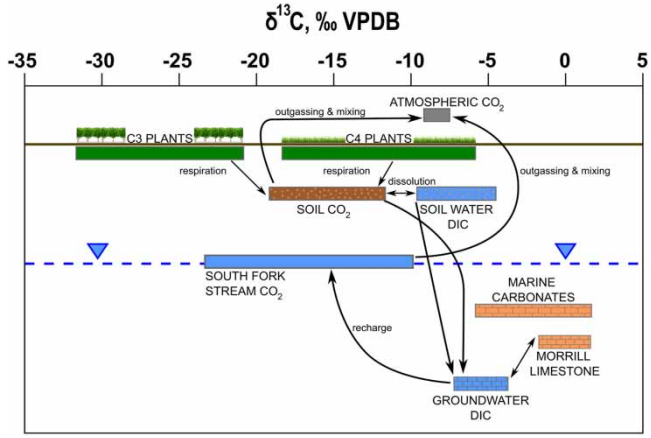

Figure 7 | Representation of stable carbon isotope ranges for carbon reservoirs at the study site.

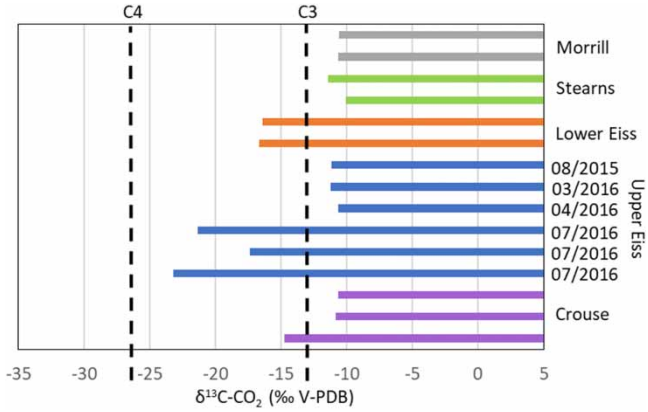

Figure 8 | Carbon isotope ratios of CO_2 efflux from stream water. Point sources are plotted for Upper Eiss (sampling month and year indicated) and Lower Eiss; stream reaches with no identified point sources include Stearns and Morrill. The lightest Crouse value is from the spring, which is just west of the stream; the other Crouse values are from downstream locations underlain by the Crouse.

Eiss Limestone locations are located in a densely wooded riparian zone. The mean δ^{13}C-CO_2 values within 1–2 m of discharge locations in stream reaches underlain by the Eiss Limestone and the Crouse Limestone were -21.0 ± 2.3‰ (V-PDB) and -14.7 ± 0.0 ‰ (V-PDB), respectively, reflecting the nearby vegetation (Figure 8).

The largest number of measurements in a single geologic unit, point sources in the Upper Eiss Limestone (Figure 8), demonstrates variable weather and climate. Moisture, as reflected by precipitation and streamflow, is a primary control, as it affects the flux direction across the groundwater–surface water interface, residence times (reactions times), and plant functioning. Further, the general direction of groundwater flow at Konza has been shown to be opposite of the streamflow direction in the Morrill, but the same as streamflow in the Eiss (Sullivan *et al.* 2020). The variation in CO_2 flux and isotopic values measured in the Eiss further illustrate the complexity of characterizing CO_2 flux in headwater streams with: (1) thin limestone aquifers, with and without point sources; (2) large interannual variations in total meteoric precipitation and in timing of meteoric precipitation; and (3) large interannual variations in stream discharge. This is consistent with the study by Duvert *et al.* (2018) who found that CO_2 evasion is heavily influenced by spatial heterogeneities in the surface and subsurface. Recent work also highlights the influence of temporal variability in hydrogeologic and hydrologic conditions on CO_2 evasion, particularly through changes in the interactions between surface and subsurface and their respective responses to meteorology (Duvert *et al.* 2018; Marx *et al.* 2018).

The difference between CO_2 flux and δ^{13}C-CO_2 collected from the Upper Eiss in 2015 and 2016 and the Crouse in 2016 illustrates the effect of hydrologic response to meteorology and limestone heterogeneity. In drier years, e.g., 2015 (preceded by an even drier year in 2014; Supplemental Table S5), groundwater residence time is longer and the buildup of CO_2 in groundwater is evidenced as higher CO_2 in point sources discharging to the stream. Higher water tables in wetter years reduce the distance between the surface and water table, with a wetter vadose zone increasing the unsaturated hydraulic conductivity, lowering groundwater residence time (Brookfield *et al.* 2017; Hatley *et al.* 2023).

6. CONCLUSIONS

This study examines the timing and extent of CO_2 transport from shallow aquifers to the atmosphere and supports findings from similar studies that headwater streams are significant contributors to local and regional carbon cycling. At Konza, 45 measurements of CO_2 efflux were taken at 18 different locations along a headwater stream. The spatial variability of CO_2 flux along the 1.1-km stream segment reflects the underlying merokarst geology and the rapid decrease in CO_2 flux downstream of point sources of discharge. Point sources, detected by water temperature, were only observed in reaches underlain by limestones; at point sources, CO_2 flux measured 2 m downstream from the point source ranged from 3 to 40% of the point-source flux, regardless of the magnitude of the point-source CO_2 flux.

The stable isotopic composition of CO_2 (δ^{13}C-CO_2) was studied as a potential tracer of groundwater influx and predictor of CO_2 efflux rate. Lower δ^{13}C-CO_2 values were often accompanied by larger CO_2 fluxes, but the inverse relationship is not predictive, likely because disequilibrium between stream CO_2 and atmospheric CO_2 is the main driver of efflux. Thus, δ^{13}C-CO_2

can be a reliable indicator of groundwater discharge into a stream where a high contrast in partial pressure of CO_2 exists between groundwater and stream water, but it is not a reliable indicator of the CO_2 efflux rate.

The large range of CO_2 fluxes and δ^{13}C-CO_2 values observed over small spatial extents reinforces the importance of point-source measurements in headwater streams, especially in those areas where karst, or other preferential flow paths, controls groundwater flow. Hence, large-scale investigations of stream degassing based on tracer tests or mass balance equations may overlook significant CO_2 contributions. The suspended chamber proved to be a simple and effective method for collecting measurements of CO_2 flux directly from the stream surface. This study provides additional reasons to consider shallow aquifers and headwater streams when accounting for carbon sinks and sources on local, regional, and global scales.

ACKNOWLEDGEMENTS

Climate and stream discharge datasets were provided by the Climate and Hydrology Database Projects (http://climhy.lternet.edu/), a partnership between the Long-Term Ecological Research program and the US Forest Service Pacific Northwest Research Station, Corvallis, Oregon. Significant funding for these data was provided by the National Science Foundation Long-Term Ecological Research program and the USDA Forest Service. B. S. N. and G. L. M. are grateful for support from the Konza Prairie LTER program (DEB-0823341 and DEB-1440484), the Geology Associates Fund of the KU Endowment Association, and the KU Department of Geology. A portion of coauthor PLS's time was supported by NSF EAR 2024388. B. S. N. thanks Mike Rawitch, Trevor Osorno, Emily Barry, Mackenzie Creamens, and Brooks Bailey for field assistance and consultation.

DATA AVAILABILITY STATEMENT

All relevant data are included in the paper or its Supplementary Information.

CONFLICT OF INTEREST

The authors declare there is no conflict.

REFERENCES

Alin, S. R., de Fátima, F. L., Rasera, M., Salimon, C. I., Richey, J. E., Holtgrieve, G. W., Krusche, A. V. & Snidvongs, A. 2011 Physical controls on carbon dioxide transfer velocity and flux in low-gradient river systems and implications for regional carbon budgets. *Journal of Geophysical Research Biogeosciences* **116**, G01009. doi:10.1029/2010JG001398.

Andrews, J. A. & Schlesinger, W. H. 2001 Soil CO_2 dynamics, acidification, and chemical weathering in a temperate forest, with experimental CO_2 enrichment. *Global Biogeochemical Cycles.* **15**, 149–162.

Atekwana, E. A. & Krishnamurthy, R. V. 1998 Seasonal variations of dissolved inorganic carbon and δ^{13}C of surface waters: Application of a modified gas evolution technique. *Journal of Hydrology* **205** (3–4), 265–278.

Atkins, M. L., Santos, I. R., Ruiz-Halpern, S. & Maher, D. T. 2013 Carbon dioxide dynamics driven by groundwater discharge in a coastal floodplain creek. *Journal of Hydrology* **493**, 30–42.

Barry, E. 2018 *Characterizing Groundwater Flow Through Merokarst, Northeast Kansas, USA*, MS thesis, *University of Kansas*Lawrence, KS, p. 118.

Battin, T. J., Kaplan, L. A., Findlay, S., Hopkinson, C. S., Marti, E., Packman, A. I., Newbold, J. D. & Sabater, F. 2009 Erratum: Biophysical controls on organic carbon fluxes in fluvial networks. *Nature Geoscience* **2** (8), 59.

Bernal, S., Cohen, M. J., Ledesma, J. L., Kirk, L., Martí, E. & Lupon, A. 2022 Stream metabolism sources a large fraction of carbon dioxide to the atmosphere in two hydrologically contrasting headwater streams. *Limnology and Oceanography*.

Brookfield, A., Macpherson, G. L. & Covington, M. 2017 Effects of changing meteoric precipitation patterns on groundwater temperature in karst environments. *Groundwater* **55** (2), 227–236.

Brown, T. L., LeMay, E. H., Bursten, B. E., Murphy, C. J. & Woodward, P. 2009 Factors affecting solubility. In: *Chemistry the Central Science* (Langford, S., Sagatys, D. & George, A. eds.), 11th edn. Pearson, p. 541.

Butman, D. & Raymond, P. A. 2011 Significant efflux of carbon dioxide from streams and rivers in the United States. *Nature Geoscience* **4** (12), 839–842.

Cernusak, L. A., Ubierna, N., Winter, K., Holtum, J. A. M., Marshall, J. D. & Farquhar, G. D. 2013 Environmental and physiological determinants of carbon isotope discrimination in terrestrial plants. *New Phytologist* **200**, 950–965. doi:10.1111/nph.12423.

Chapelle, F. H. 2000 The significance of microbial processes in hydrogeology and geochemistry. *Hydrogeology Journal* **8** (1), 41–46.

Charlton, S. R., Macklin, C. L. & Parkhurst, D. L. 1997 *PHREEQCI, a Graphical User Interface for the Geochemical Computer Program PHREEQC*. U.S. Department of the Interior, U.S. Geological Survey, Lakewood, CO.

Chen, Z., Auler, A. S., Bakalowicz, M., Drew, D., Griger, F., Hartmann, J., Jiang, G., Moosdorf, N., Richts, A., Stevanovic, Z. & Veni, G. 2017 The world karst aquifer mapping project: Concept, mapping procedure and map of Europe. *Hydrogeology Journal* **25** (3), 771–785.

Cisneros-Dozal, L. M., Trumbore, S. & Hanson, P. J. 2006 Partitioning sources of soil-respired CO_2 and their seasonal variation using a unique radiocarbon tracer. *Global Change Biology* **12** (2), 194–204.

Cole, J. J. & Caraco, N. F. 1998 Atmospheric exchange of carbon dioxide in a low-wind oligotrophic lake measured by the addition of SF_6. *Limnology and Oceanography* **43** (4), 647–656.

Cole, J. J., Prairie, Y. T., Caraco, N. F., McDowell, W. H., Tranvik, L. J., Striegl, R. G., Duarte, C. M., Kortelainen, P., Downing, J. A., Middelburg, J. J. & Melack, J. 2007 Plumbing the global carbon cycle: Integrating inland waters into the terrestrial carbon budget. *Ecosystems* **10** (1), 172–185.

Cole, J. J., Bade, D. L., Bastviken, D., Pace, M. L. & Van de Bogert, M. 2010 Multiple approaches to estimating air-water gas exchange in small lakes. *Limnology and Oceanography: Methods* **8**, 285–293.

Crawford, J. T., Striegl, R. G., Wickland, K. P., Dornblaser, M. M. & Stanley, E. H. 2013 Emissions of carbon dioxide and methane from a headwater stream network of interior Alaska. *Journal of Geophysical Research: Biogeosciences* **118** (2), 482–494.

Crawford, J. T., Lottig, N. R., Stanley, E. H., Walker, J. F., Hanson, P. C., Finlay, J. C. & Striegl, R. G. 2014 CO_2 and CH_4 emissions from streams in a lake-rich landscape: Patterns, controls, and regional significance. *Global Biogeochemical Cycles* **28** (3), 197–210.

Deirmendjian, L. & Abril, G. 2018 Carbon dioxide degassing at the groundwater-stream-atmosphere interface: Isotopic equilibration and hydrological mass balance in a sandy watershed. *Journal of Hydrology* **558**, 129–143.

Deirmendjian, L., Loustau, D., Augusto, L., Lafont, S., Chipeaux, C., Poirier, D. & Abril, G. 2018 Hydro-ecological controls on dissolved carbon dynamics in groundwater and export to streams in a temperate pine forest. *Biogeosciences* **15** (2), 669–691.

Demars, B. O. L. & Manson, J. R. 2013 Temperature dependence of stream aeration coefficients and the effect of water turbulence: A critical review. *Water Research* **47** (1), 1–15.

Dinsmore, K. J., Wallin, M. B., Johnson, M. S., Billett, M. F., Bishop, K., Pumpanen, J. & Ojala, A. 2013 Contrasting CO_2 concentration discharge dynamics in headwater streams: A multi-catchment comparison. *Journal of Geophysical Research: Biogeosciences* **118** (2), 445–461.

Doctor, D. H., Kendall, C., Sebestyen, S. D., Shanley, J. B., Ohte, N. & Boyer, E. W. 2008 Carbon isotope fractionation of dissolved inorganic carbon (DIC) due to outgassing of carbon dioxide from a headwater stream. *Hydrological Processes: An International Journal* **22** (14), 2410–2423.

Dodds, W. K. 2021 ASD02 stream discharge measured at the flumes on watershed N04D at Konza Prairie. *Environmental Data Initiative*. http://dx.doi.org/10.6073/pasta/43cac10952a6115c1df8882fa2134a7c.

Duvert, C., Butman, D. E., Marx, A., Ribolzi, O. & Hutley, L. B. 2018 CO_2 evasion along streams driven by groundwater inputs and geomorphic controls. *Nature Geoscience* **11**, 813–818.

Hatley, C. M, Armijo, Andrews, B., Anhold, K., Nippert, C. & Kirk, J. B., M. F. 2023 Intermittent streamflow generation in a merokarst headwater catchment. *Environmental Science: Advances* **2**, 115–131.

Hayden, B. P. 1998 Regional climate and the distribution of tallgrass prairie. In: *Grassland Dynamics Long-Term Ecological Research in Tallgrass Prairie* (Knapp, A. K., Briggs, J. M., Hartnett, D. C. & Collins, S. L. eds). Oxford University Press, New York, NY, pp. 19–34.

Hélie, J. F., Hillaire-Marcel, C. & Rondeau, B. 2002 Seasonal changes in the sources and fluxes of dissolved inorganic carbon through the St. Lawrence River – Isotopic and chemical constraint. *Chemical Geology* **186** (1–2), 117–138.

Hendry, M. J., Lawrence, J. R., Zanyk, B. N. & Kirkland, R. 1993 Microbial production of CO_2 in unsaturated geologic media in a mesoscale model. *Water Resources Research* **29** (4), 973–984.

Hope, D., Palmer, S. M., Billett, M. F. & Dawson, J. J. 2001 Carbon dioxide and methane evasion from a temperate peatland stream. *Limnology and Oceanography* **46** (4), 847–857.

Horgby, Å., Segatto, P. L., Bertuzzo, E., Lauerwald, R., Lehner, B., Ulseth, A. J., Vennemann, T. W. & Battin, T. J. 2019 Unexpected large evasion fluxes of carbon dioxide from turbulent streams draining the world's mountains. *Nature Communications* **10** (1), 1–9.

Hotchkiss, E. R., Hall Jr, R. O., Sponseller, R. A., Butman, D., Klaminder, J., Laudon, H., Rosvall, M. & Karlsson, J. J. N. G. 2015 Sources of and processes controlling CO 2 emissions change with the size of streams and rivers. *Nature Geoscience* **8** (9), 696–699.

Johnson, M. S., Lehmann, J., Riha, S. J., Krusche, A. V., Richey, J. E., Ometto, J. P. H. & Couto, E. G. 2008 CO_2 efflux from Amazonian headwater streams represents a significant fate for deep soil respiration. *Geophysical Research Letters* **35**, 17.

Karim, A. & Veizer, J. 2000 Weathering processes in the Indus River Basin: Implications from riverine carbon, sulfur, oxygen, and strontium isotopes. *Chemical Geology* **170** (1–4), 153–177.

Kessler, T. J. & Harvey, C. F. 2001 The global flux of carbon dioxide into groundwater. *Geophysical Research Letters* **28** (2), 279–282.

Kuzyakov, Y. & Domanski, G. 2000 Carbon input by plants into the soil. Review. *Journal of Plant Nutrition and Soil Science* **163** (4), 421–431.

Lee, K. Y., van Geldern, R. & Barth, J. A. 2021 Extreme gradients in CO_2 losses downstream of karstic springs. *Science of the Total Environment* **778**, 146099.

Li, M., Peng, C., Zhang, K., Xu, L., Wang, J., Yang, Y., Li, P., Liu, Z. & He, N. 2021 Headwater stream ecosystem: An important source of greenhouse gases to the atmosphere. *Water Research* **190**, 116738.

Maas, B. J. & Wicks, C. M. 2017 CO_2 outgassing from spring waters. *Aquatic Geochemistry* **23** (1), 53–60. doi:10.1007/s10498-016-9302-6.

MacIntyre, S., Wanninkhof, R. & Chanton, J. 1995 Trace gas exchange across the air-water interface in freshwater and coastal marine environments. In: *Biogenic Trace Gases: measuring Emissions From Soil and Water* (Matson RA & Harris RC, eds.). Blackwell Science, Oxford, pp. 52–97.

Macpherson, G. L. & Sophocleous, M. 2004 Fast ground-water mixing and basal recharge in an unconfined, alluvial aquifer, Konza LTER Site, Northeastern Kansas. *Journal of Hydrology* **286** (1–4), 271–299.

Macpherson, G. L. & Sullivan, P. L. 2019 Watershed-scale chemical weathering in a merokarst terrain, northeastern Kansas, USA. *Chemical Geology* **527**, 118988.

Macpherson, G. L. 1996 Hydrogeology of thin-bedded limestones – The Konza Prairie LTER site, northeastern Kansas. *Journal of Hydrology* **186** (1–4), 191–229.

Macpherson, G. L. 2009 CO_2 distribution in groundwater and the impact of groundwater extraction on the global C cycle. *Chemical Geology* **264** (1–4), 328–336.

Macpherson, G. L. 2020 AGW03 Konza Prairie Long-term high frequency groundwater level and temperature from wells on n04d. *Environmental Data Initiative*. https://doi.org/10.6073/pasta/6faaf55025f355358510260e0b9e4fb7.

Macpherson, G. L., Roberts, J. A., Blair, J. M., Townsend, M. A., Fowle, D. A. & Beisner, K. R. 2008 Increasing shallow groundwater CO_2 and limestone weathering, Konza Prairie, USA. *Geochimica et Cosmochimica Acta* **72** (23), 5581–5599.

Marx, A., Dusek, J., Jankovec, J., Sanda, M., Vogel, T., Van Geldern, R., Hartmann, J. & Barth, J. A. C. 2017 A review of CO_2 and associated carbon dynamics in headwater streams: A global perspective. *Reviews of Geophysics* **55** (2), 560–585.

Marx, A., Conrad, M., Aizinger, V., Prechtel, A., van Geldern, R. & Barth, J. A. 2018 Groundwater data improve modelling of headwater stream CO_2 outgassing with a stable DIC isotope approach. *Biogeosciences* **15** (10), 3093–3106.

Mayorga, E., Aufdenkampe, A. K., Masiello, C. A., Krusche, A. V., Hedges, J. I., Quay, P. D., Richey, J. E. & Brown, T. A. 2005 Young organic matter as a source of carbon dioxide outgassing from Amazonian rivers. *Nature* **436** (7050), 538–541.

Meals, D. W. & Dressing, S. A. 2008 Surface water flow measurement for water quality monitoring. EPA Tech Notes. Available from: https://www.epa.gov/sites/production/files/2016-05/documents/tech_notes_3_dec2013_surface_flow.pdf.

Mohammadi, Z., Vaselli, O., Muchez, P., Claes, H., Capezzuoli, E. & Swennen, R. 2020 Hydrogeochemistry, stable isotope composition and geothermometry of CO_2-bearing hydrothermal springs from Western Iran: Evidence for their origin, evolution and spatio-temporal variations. *Sedimentary Geology* **404**, 105676. Available from: https://www.sciencedirect.com/science/article/pii/S0037073820300919.

Monger, H. C., Kraimer, R. A., Khresat, S. E., Cole, D. R., Wang, X. & Wang, J. 2015 Sequestration of inorganic carbon in soil and groundwater. *Geology* **43** (5), 375–378.

Müller, D., Warneke, T., Rixen, T., Müller, M., Jamahari, S., Denis, N., Mujahid, A. & Notholt, J. 2015 Lateral carbon fluxes and CO_2 outgassing from a tropical peat-draining river. *Biogeosciences* **12** (20), 5967–5979.

Nadeau, T. L. & Rains, M. C. 2007 Hydrological connectivity between headwater streams and downstream waters: How science can inform policy 1. *JAWRA Journal of the American Water Resources Association* **43** (1), 118–133.

Nippert, J. 2017 AWE01 meteorological data from the konza prairie headquarters weather station. *Konza Prairie Long Term Ecological Research (LTER) Program*. http://dx.doi.org/10.6073/pasta/743c6b205e38a087bc54925ed258f549.

Nippert, J. B. & Knapp, A. K. 2007 Soil water partitioning contributes to species coexistence in tallgrass prairie. *Oikos* **116** (6), 1017–1029.

Norwood, B. N. 2020 *Flux and Stable Isotope Fractionation of CO_2 in a Headwater Stream*. MS Thesis, University of Kansas, KS, p. 92.

Nosrati, K., Collins, A. L. & Fiener, P. 2020 Using catchment characteristics to model seasonality of dissolved organic carbon fluxes in semi-arid mountainous headwaters. *Environmental Monitoring and Assessment* **192**, 674.

NRCS (National Resources Conservation Service) 2006 Soils in Riley and Geary Counties, Kansas. NRCS, Accessed Online 11 February 006, 11:15 am.

Pomes, M. L. 1995 *A Study of the Aquatic Humic Substances and Hydrogeology in a Prairie Watershed–Use of Humic Material as a Tracer of Recharge Through Soils*. *PhD dissertation*, University of Kansas, KS, p. 296.

Ranson, M. D., Rice, C. W., Todd, T. C., Wehmueller, W. A., 1998 Soils and soil biota. In: *Grassland Dynamics – Long-Term Ecological Research in Tallgrass Prairie* (Knapp, A. K., Briggs, J. M., Hartnett, D. C. & Collins, S. L., eds). Oxford University Press, New York, pp. 48–68.

Rawitch, M., Macpherson, G. L. & Brookfield, A. 2019 Exploring methods of measuring CO_2 degassing in headwater streams. *Sustainable Water Resources Management* **5** (4), 1765–1779.

Rawitch, M. J., Macpherson, G. L. & Brookfield, A. E. 2021 The validity of floating chambers in quantifying CO_2 flux from headwater streams. *Journal of Water and Climate Change* **12** (2), 453–468. doi: 10.2166/wcc.2020.199.

Sand-Jensen, K. & Staehr, P. A. 2012 CO_2 dynamics along Danish lowland streams: water–air gradients, piston velocities and evasion rates. *Biogeochemistry* **111** (1), 615–628.

Schade, J. D., Bailio, J. & McDowell, W. H. 2016 Greenhouse gas flux from headwater streams in New Hampshire, USA: Patterns and drivers. *Limnology and Oceanography* **61**, S165–S174.

Schlesinger, W. H. & Lichter, J. 2001 Limited carbon storage in soil and litter of experimental forest plots under increased atmospheric CO_2. *Nature* **411** (6836), 466–469.

Schlesinger, W. H. & Melack, J. M. 1981 Transport of organic carbon in the world's rivers. *Tellus* **33** (2), 172–187.

Striegl, R. G., Dornblaser, M. M., McDonald, C. P., Rover, J. R. & Stets, E. G. 2012 Carbon dioxide and methane emissions from the Yukon River system. *Global Biogeochemical Cycles* **26** (4). https://doi.org/10.1029/2012GB004306.

Sullivan, P., Macpherson, L., Martin, G. L. & Price, J. B., R. M. 2019 Evolution of carbonate and karst critical zones. *Chemical Geology* **527**, 119223.

Sullivan, P. L., Zhang, C., Behm, M., Zhang, F. & Macpherson, G. L. 2020 Toward a new conceptual model for groundwater flow in merokarst systems: Insights from multiple geophysical approaches. *Hydrological Processes* **34** (24), 4697–4711. doi: 10.1002/hyp.13898.

Taylor, C. B. & Fox, V. J. 1996 An isotopic study of dissolved inorganic carbon in the catchment of the Waimakariri River and deep ground water of the North Canterbury Plains, New Zealand. *Journal of Hydrology* **186** (1–4), 161–190.

Tsypin, M. & Macpherson, G. L. 2012 The effect of precipitation events on inorganic carbon in soil and shallow groundwater, Konza Prairie LTER Site, NE Kansas, USA. *Applied Geochemistry* **27** (12), 2356–2369. doi:10/1016/j.apgeochem.2012.07.008.

Twiss, P. C. 1988 Beattie Limestone (Lower Permian) of Eastern Kansas. Centennial Field Guide Volume 4: South-Central Section of the Geological Society of America: 35–41.

USGS 2016 How Streamflow Is Measured: The Discharge Measurement. How Streamflow Is Measured. N.p., n.d. Web. Jan. 2016.

Veach, A. M., Dodds, W. K. & Skibbe, A. 2014 Fire and grazing influences on rates of riparian woody plant expansion along grassland streams. *PloS One* **9** (9), e106922.

Venkiteswaran, J. J., Schiff, S. L. & Wallin, M. B. 2014 Large carbon dioxide fluxes from headwater boreal and sub-boreal streams. *PloS One* **9** (7), e101756.

Wallin, M. B., Audet, J., Peacock, M., Sahlée, E. & Winterdahl, M. 2020 Carbon dioxide dynamics in an agricultural headwater stream driven by hydrology and primary production. *Biogeosciences* **17** (9), 2487–2498.

Wang, C., Guo, L., Li, Y. & Wang, Z. 2012 Systematic comparison of C3 and C4 plants based on metabolic network analysis. *BMC Systems Biology* **6**(2), S9.

Wanninkhof, R. 2014 Relationship between wind speed and gas exchange over the ocean revisited. *Limnology and Oceanography: Methods* **12** (6), 351–362.

Weary, D. J. & Doctor, D. H. 2014 *Karst in the United States: A Digital map Compilation and Database*. US Department of the Interior, US Geological Survey, Reston, VA, USA, p. 26.

Wen, H., Sullivan, P. L., Macpherson, G. L. & Li, L. 2021 Deepening roots enhance carbonate weathering by amplifying CO_2-rich recharge. *Biogeosciences* **18**, 55–75.

Winter, T. C., Harvey, J. W., Franke, O. L. & Alley, W. M. 1998 *Ground Water and Surface Water: US Department of the Interior*. US Geological Survey. https://doi.org/10.3133/cir1139

Yang, C., Telmer, K. & Veizer, J. 1996 Chemical dynamics of the 'St. Lawrence' riverine system: δD_{H2O}, $\delta^{18}O_{H2O}$, $\delta^{13}C_{DIC}$, $\delta^{34}S_{sulfate}$, and dissolved $^{87}sr/^{86}sr$. *Geochimica et Cosmochimica Acta* **60** (5), 851–866.

First received 30 January 2023; accepted in revised form 7 May 2023. Available online 19 May 2023